

Maximum-likelihood based range-dependence compensation for coherent multistatic STAP radar

Xavier Neyt, Marc Acheroy
 Electrical Engineering Dept.,
 Royal Military Academy,
 Belgium
 Xavier.Neyt@rma.ac.be
 Marc.Acheroy@rma.ac.be

Jacques G. Verly
 Dept. of Electrical Engineering
 and Computer Science,
 University of Liège,
 Belgium
 Jacques.Verly@ulg.ac.be

Abstract— We study the performance of space-time adaptive processing (STAP) applied to coherent multistatic radar. The radars we consider are passive (receive only) but are synchronized in order to allow coherent processing of the data among the different radars. One of the major benefit of multistatism is that the full velocity vectors of the targets can be measured. Furthermore, we study the feasibility of estimating the clutter covariance matrix, required to compute the STAP filter. We show that range-dependence effects cause the usual sample matrix inversion (SMI) scheme to fail and we propose a method able to cope with arbitrary multistatic geometries.

I. INTRODUCTION

Multistatic radars have recently gained a lot of interest [1]–[3]. In [4], [5], multistatic radars are shown to increase the localization accuracy of the targets. In [6], [7], the benefit of non-coherent multistatic radar processing is analyzed. However, they rely on the knowledge of the $i+n$ covariance matrix but do not address the problem of its estimation.

The multistatic radar we consider consists in several non collocated mutually coherent bistatic radars. In particular, we consider one transmitter and several receivers. The transmit platform, possibly moving, illuminates the whole area of interest. The (moving) receive platforms, for instance UAVs, each carry an antenna array of arbitrary shape with several channels. The objective of the system is to detect ground moving targets buried in clutter signal.

The scenario considered for the illustrations is depicted in Fig. 1. The arrows indicate the velocity vector of each receiver. Each oval represents the isorange for each bistatic radar at the range of the target.

We assume that the receivers of each platform are synchronized and that the response of the matched filter performing the pulse compression on each platform is delayed such that the response of the target arrives in phase at a reference channel on each platform, in a similar way as what is described in [8]. We also assume that the target consists in one single scatterer, such that the target echo can be considered coherent regardless of the look angle. Both assumptions are in line with what is done in [4], [5].

The paper is organized as follows. In Section II, we review the signal modeling and the particularities of STAP for multistatic radar. In Section III, we present the clutter power

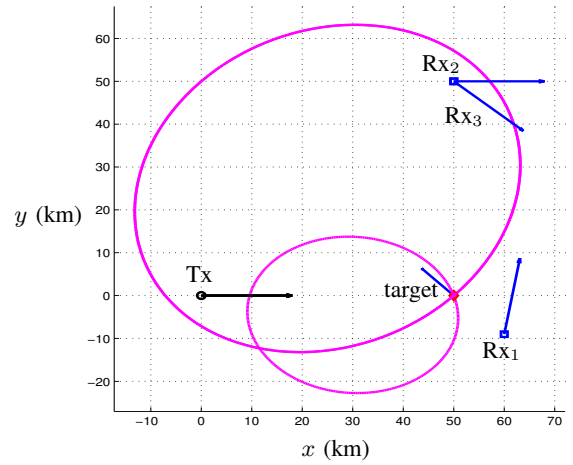


Fig. 1. Scenario considered in the paper.

spectrum (PS) locus in the case of multistatic radar, while the range-dependency of the clutter signal statistics is analyzed in Section IV. Finally, in Section V we propose the generalization of a range-dependence compensation method able to cope with arbitrary multistatic radar. Section VI presents end-to-end results and Section VII concludes.

II. SIGNAL MODELING

Platform p carry N_p receive channels with arbitrary but known locations, and there is a total of $N = \sum_{p=1}^P N_p$ channels where P is the total number of platforms. At each receive channel, the signal is matched filtered and sampled in order to produce M samples in time. The sampling of the matched filtering output is performed such that the relative phase for a stationary reflector that would be located at the target position is constant at the reference receive channel of each platform.

Let us denote the lexically-ordered $N_p \times M$ space-time samples received at platform p by \mathbf{y}_p . The received space-time samples at all channels of all platforms can be stacked and noted

$$\mathbf{y} = [\mathbf{y}_1^T, \mathbf{y}_2^T, \dots, \mathbf{y}_P^T]^T. \quad (1)$$

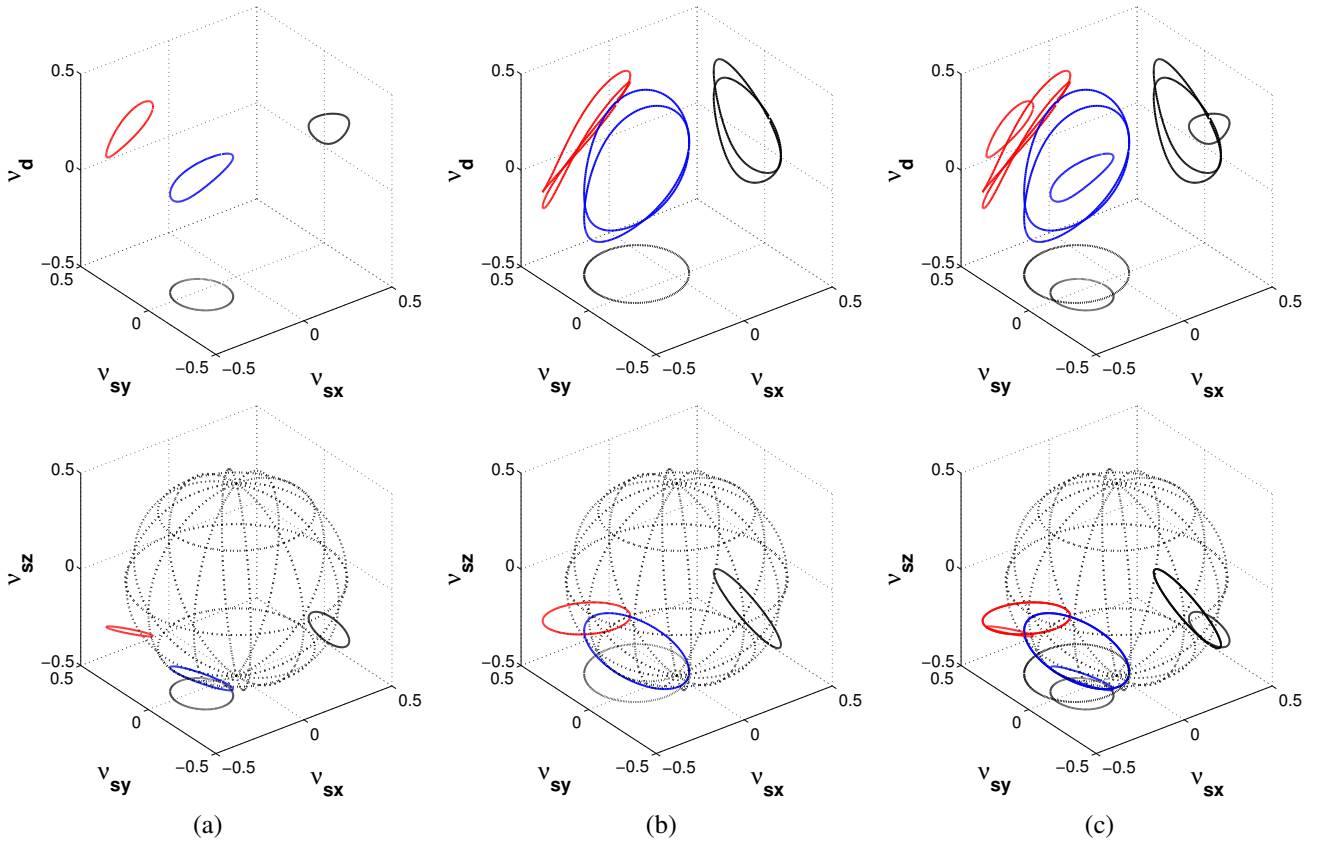


Fig. 2. Clutter power spectrum locus corresponding to (a) the receivers on platform Rx_1 alone, (b) the receivers on platform Rx_2 and Rx_3 and (c) the combination of all the receivers on all platforms.

In the presence of a target located at \vec{r}_t , the received signal can be modeled as

$$\mathbf{y} = \alpha \mathbf{s}(\boldsymbol{\theta}(\vec{r}_t)) + \mathbf{y}^{i+n} \quad (2)$$

where α is the deterministic complex amplitude of the target signal. Since we consider the target coherent among the different receivers, α is identical for all receive platforms. Similarly to (1), $\mathbf{s}(\boldsymbol{\theta})$ is the stacking of the P steering vectors $\mathbf{s}_p(\boldsymbol{\theta}_p)$ corresponding to each individual bistatic radar

$$\mathbf{s}(\boldsymbol{\theta}) = [\mathbf{s}_1^T(\boldsymbol{\theta}_1), \mathbf{s}_2^T(\boldsymbol{\theta}_2), \dots, \mathbf{s}_P^T(\boldsymbol{\theta}_P)]^T. \quad (3)$$

The vector $\boldsymbol{\theta}$ is the vector of parameters that governs the steering vector and is formed by the stacking of P vectors of parameters corresponding to each bistatic radar $\boldsymbol{\theta} = [\boldsymbol{\theta}_1^T, \boldsymbol{\theta}_2^T, \dots, \boldsymbol{\theta}_P^T]^T$. Each vector of parameters $\boldsymbol{\theta}_p$ contains the elevation angle θ and the azimuth angle φ of the look direction of the corresponding steering vector. Note that, in a multistatic setup, the vector of parameters $\boldsymbol{\theta}_p$ is typically different for each bistatic radar, this dependence being indicated by the subscript p . The notation $\boldsymbol{\theta}(\vec{r}_t)$ denotes the vector of parameters such that the steering vector of each bistatic radar looks towards the location \vec{r}_t , in this case the location of the target.

The unwanted interference (clutter) plus noise ($i+n$) signal component is denoted by \mathbf{y}^{i+n} and can be expressed as the stacking of the $i+n$ signal component measured by each bistatic

radar as in (1)

$$\mathbf{y}^{i+n} = [\mathbf{y}_1^{i+nT}, \mathbf{y}_2^{i+nT}, \dots, \mathbf{y}_P^{i+nT}]^T. \quad (4)$$

The $i+n$ signal component of each bistatic radar can be modeled as [9], [10]

$$\mathbf{y}_p^{i+n} = \sum_{i=0}^{N_c} a_{p_i} c_{p_i} \mathbf{s}_p(\boldsymbol{\theta}_{p_i}) + \mathbf{n}_p, \quad (5)$$

where the sum is conducted over N_c clutter patches spread along the isorange. The coefficients a_{p_i} denote the (complex) reflectivity of clutter patch i along the isorange, c_{p_i} is a known factor that groups the geometric terms of the radar equation (range attenuation, antenna radiation pattern, ...), $\mathbf{s}_p(\boldsymbol{\theta}_{p_i})$ is the steering vector of the bistatic radar p that looks in the direction of clutter patch i denoted $\boldsymbol{\theta}_{p_i}$ and \mathbf{n} is the thermal noise. It should be noted that $\boldsymbol{\theta}_{p_i}$ depend on the isorange considered and the isorange considered depends on the range of interest, which, in the case of (2), is the range of the target determined by its location \vec{r}_t . Equation (5) can be rewritten as

$$\mathbf{y}_p^{i+n} = S_{cp} \mathbf{a}_p + \mathbf{n}_p, \quad (6)$$

where $S_{cp} = [c_{p_1} \mathbf{s}_p(\boldsymbol{\theta}_{p_1}), c_{p_2} \mathbf{s}_p(\boldsymbol{\theta}_{p_2}), \dots, c_{p_{N_c}} \mathbf{s}_p(\boldsymbol{\theta}_{p_{N_c}})]$ and $\mathbf{a}_p = [a_{p_1}, \dots, a_{p_{N_c}}]$. Similarly, (4) can be rewritten as

$$\mathbf{y}^{i+n} = S_c \mathbf{a} + \mathbf{n}, \quad (7)$$

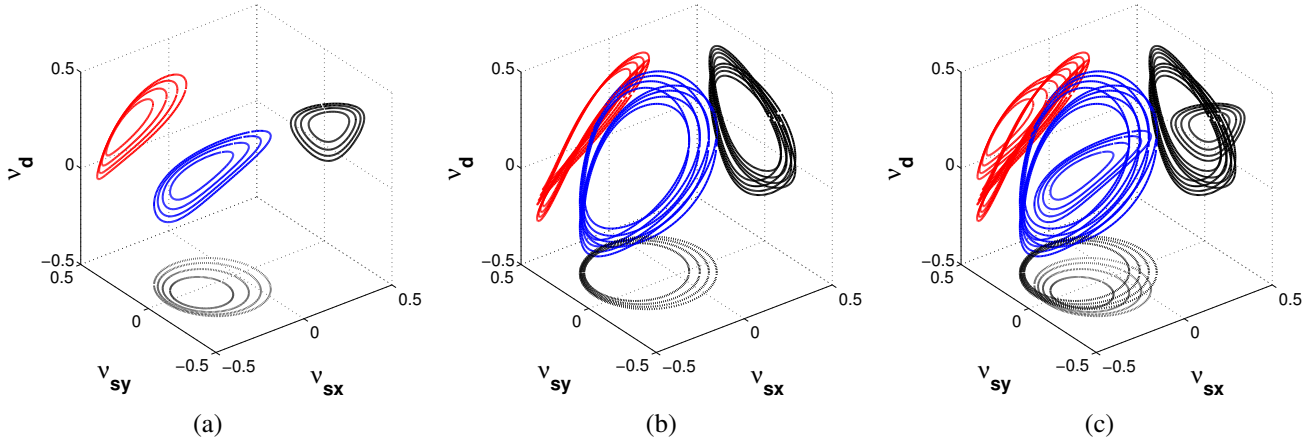


Fig. 3. Clutter PS locus (and its projection on the vertical and horizontal planes) at different ranges around the target's range and corresponding to (a) the bistatic radar Tx-Rx₁ alone, (b) the bistatic radar Tx-Rx₂ and Tx-Rx₃ and (c) the combination of all the bistatic radars.

where $S_c = [S_{c_1}^T, \dots, S_{c_P}^T]^T$ and $\mathbf{a} = [\mathbf{a}_1^T, \dots, \mathbf{a}_P^T]^T$.

The optimum STAP filter is given by

$$\mathbf{w} = \gamma R^{-1} \mathbf{s}(\theta(\mathbf{r}_t)), \quad (8)$$

where γ is a constant and R is the i+n covariance matrix

$$R = E\{\mathbf{y}_{i+n} \mathbf{y}_{i+n}^\dagger\}. \quad (9)$$

The optimum estimate of α is obtained by computing

$$z = \mathbf{w}^\dagger \mathbf{y}. \quad (10)$$

The received clutter signal results from reflection by clutter patches located along an isorange on the ground. As illustrated in Fig. 1, in general, the isoranges of different bistatic radars will be different. Hence, in general, the clutter signal component present in the space-time samples of different receive platforms will be uncorrelated¹ as noted in [6]. In this case, the covariance matrix R has a block-diagonal structure and its inverse also has a block-diagonal structure with each block being the inverse of the corresponding block in the covariance matrix. Equation (10) thus reduces to the coherent summation of contributions obtained from each receive platform.

However, if the isoranges corresponding to two different bistatic radars overlap, correlation between the clutter components cannot be excluded. This case is illustrated in Fig. 1, where the platforms Rx_2 and Rx_3 are so close to each other that the isoranges totally overlap. Notice that, since each receive platform might have a different velocity, two nearly collocated platforms are not strictly equivalent to a phased array. This is where a coherent multistatic radar differs from the coherent combination of the output of several bistatic radar.

III. CLUTTER POWER SPECTRUM

The power spectrum (PS) of the clutter offers a powerful means to analyze the behavior of the clutter signal. Let us first review the 4D clutter PS locus introduced in [11]. The clutter signal results from reflections from clutter patches along the

¹Possible correlation where the isoranges intersect is neglected as the look-angle will in general be very different.

isorange on the ground. The signal from each clutter patch will be seen by the array on a single receive platform as a plane wave with a particular direction of arrival (DOA) and with a particular Doppler frequency. The DOA can be measured in terms of the 3 spatial frequencies corresponding to the 3D spatial coordinate system. The clutter PS locus is thus defined in a 4D space and can be thought of as if the isorange was imaged in the 4D spectral domain. The concept of clutter PS locus can be extended to several bistatic radars, but, as noted in [12], its interpretation is less straightforward. The 4D clutter PS locus of different combinations of the bistatic radars in the case of the scenario of Fig. 1 is represented in Fig. 2 as two 3D projections. Figure 2(a) presents the 4D clutter PS locus of a single bistatic radar, leading to a single 4D curve. Figure 2(b) presents the 4D clutter PS locus of two bistatic radars with receive platforms located close to each other but having a different velocity vector, leading to two different curves that only differ in Doppler frequency. As can be seen on the lower graph of this figure, the clutter PS locus of these two bistatic radars are superimposed in the spatial domain indicating that the clutter is seen with similar spatial frequencies. Finally, Fig. 2(c) presents the 4D clutter PS locus of all the bistatic radars considered in our scenario. This figure is a superposition of Figs. 2(a) and (b).

The formal link between the 4D clutter PS locus and the 4D clutter PS is detailed in [11]. We can summarize it by saying that the clutter PS energy is located around the clutter PS locus. This is why the clutter PS locus is such a powerful tool to understand the behavior of the clutter signal.

IV. RANGE DEPENDENCY

The computation of the STAP filter (8) requires an estimate of the i+n covariance matrix R . This estimate is typically obtained by averaging estimates obtained at ranges around the range of interest [?], [10], [13]. This method provides an unbiased estimation of the true covariance matrix only if the averaged estimates are independent and identically distributed (IID). The fact that the space-time snapshots at different ranges

are not IID is essentially due to a geometry-induced range-dependence effect. The range dependence of the clutter PS locus for the considered scenario is depicted in Fig. 3. The range dependence of the clutter PS locus is an indication of the range dependence of the clutter PS. Averaging clutter covariance matrix estimates obtained at different ranges will “smear” out the clutter PS along the clutter PS locus and bias the covariance-matrix estimate.

V. RANGE-DEPENDENCE COMPENSATION

We now present a generalization to multistatic STAP of the method presented in [14]. This method is based on the maximum likelihood (ML) estimation of the scattering coefficients \mathbf{a} of (7) in a Bayesian framework. From these values, an estimate of the $i+n$ covariance matrix can be obtained using (7) and (9)

$$R = S_c A S_c^\dagger + \sigma^2 I \quad (11)$$

where $A = \text{diag}\{\tilde{a}_{1_1}^2, \dots, \tilde{a}_{P_{N_c}}^2\}$ with $\tilde{a}_{p_i}^2 = E\{|a_{p_i}|^2\}$ and σ^2 is the variance of the thermal noise.

From [14], the ML estimate of \mathbf{a} can be obtained by

$$\mathbf{a} = W^\dagger \mathbf{y}^{i+n} \quad (12)$$

where

$$W^\dagger = (S_c^\dagger R_n^{-1} S_c + R_a^{-1})^{-1} S_c^\dagger R_n^{-1} \quad (13)$$

with R_n the covariance of the thermal noise, assumed white Gaussian, with

$$R_n = \sigma^2 I, \quad (14)$$

and R_a containing the a priori knowledge we have about \mathbf{a} . Since \mathbf{a} represent a single realization of the complex amplitude of the signal scattered by the clutter, we will assume it is independent and complex-Gaussian distributed [15], [16] and take R_a proportional to the identity matrix.

This method is very similar to that of [17], where a least-squares (LS) solution is obtained with

$$W^\dagger = (S_c^\dagger S_c)^{-1} S_c^\dagger. \quad (15)$$

However, due to the lack of the regularization term R_a^{-1} in the LS solution, it only exists if $S_c^\dagger S_c$ has full rank. This means that the number of clutter patches N_c considered in the model (5) must be smaller than or equal to the rank of $S_c^\dagger S_c$. This approach requires an ad-hoc method to estimate the number of clutter patches N_c . In our approach, by using a regularization term, the exact value of N_c is not critical as long as the number of clutter patches is sufficient so that (5) accurately approximates the underlying continuous clutter integral [9].

We will now briefly analyze the performance of this estimator. A more detailed analysis and a comparison of this method in the case of a bistatic configuration is presented in [14]. By repeating the estimation of \mathbf{a} at ranges around the range of interest, a map of the coefficients \mathbf{a} is obtained. Figure 4 depicts the amplitude of the estimated scattering coefficients $|a_{1_i}|$ for the bistatic radar Tx-Rx₁ in the case of a simulated homogeneous ground cover. The value of $|a_{1_i}|$

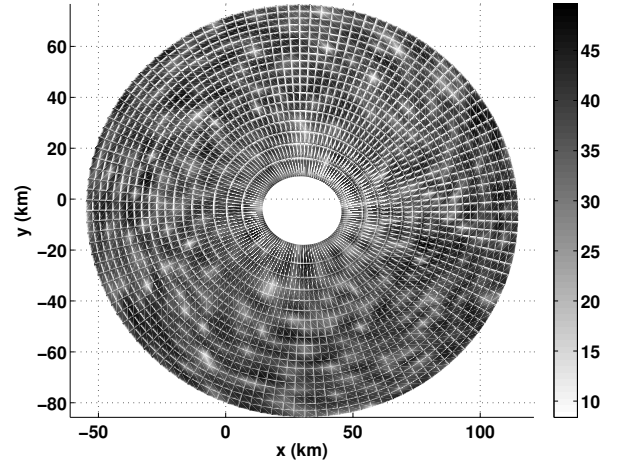


Fig. 4. Estimated clutter reflectivity $|a_{1_i}|$ at all ranges (in dB).

are depicted as a function of their actual location on the ground. Due to speckle [16], the estimated values will exhibit random variations. In fully-developed speckle, the value of the amplitude of the scattering coefficients $|\mathbf{a}|$ would be Rayleigh-distributed [15], [16]. The histogram of the amplitude of the estimated scattering coefficients $|a_{1_i}|$ can be compared with the theoretical distribution in Fig. 5. As can be seen, an excellent match is obtained.

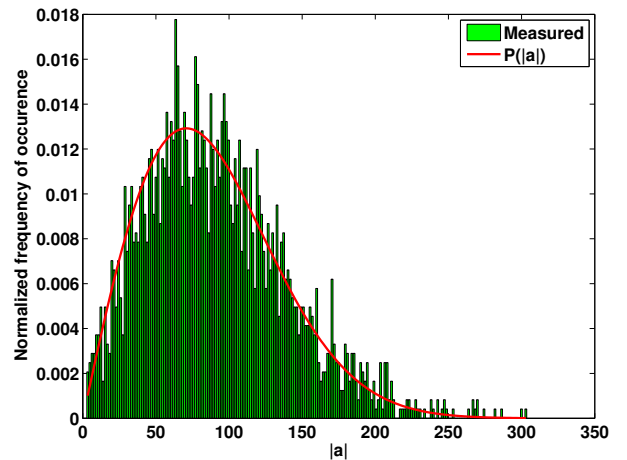


Fig. 5. Comparison of the obtained scattering coefficient amplitude distribution with the Rayleigh-distributed theoretical model $P(|a_{1_i}|)$.

An estimate of \tilde{a}_{p_i} at the range of interest can be obtained by performing a spatial averaging of $|\mathbf{a}_p|^2$ around that range. It should be stressed that the map of the estimated ground scattering coefficient obtained exhibits exactly the same characteristics as for SAR single-look complex (SLC) images. Hence, the classical multilooking methods can be applied. For instance, in order to preserve the structure possibly present in the clutter reflectivity map and due to the ground cover inhomogeneity, more sophisticated spatial filtering methods such as [18] could be used.

It should be noted that this method assumes perfect knowledge of the configuration parameters (Tx and Rx locations and velocities, antenna array element positions, ...) to be able to compute the multistatic space-time steering vectors.

The estimation of the coefficients \mathbf{a}_p needs to be done individually for each bistatic radar unless their clutter is correlated. This is the case, for instance, in the scenario we considered in this paper, with Rx₂ and Rx₃: \mathbf{a}_2 and \mathbf{a}_3 will be identical.

If several bistatic radars are considered, different overlapping maps of $|a_p|$ would typically be obtained. The values of $|a_{p_i}|^2$ at the same location obtained by different bistatic radars may not simply be averaged. Indeed, the scattering coefficients depend in a very subtle way on the geometry (incidence angle) but also for instance on the surface roughness. Inversion using geophysical models such as [15], [19] for soil, [20], [21] for sea-ice, and [22] for ocean surface could be attempted. However, besides the fact that very few bistatic model exist and without taking into account the feasibility of the inversion, it would be very demanding for a relatively small gain.

We now summarize the method, which consists in 3 steps: (a) an analysis step, where the ground scattering coefficients \mathbf{a} is estimated at ranges around the range of interest; (b) an averaging step where the clutter reflectivity $|a_{p_i}|^2$ is spatially averaged to yield $\tilde{a}_{p_i}^2$. At this step, inhomogeneities in the ground cover can be taken into account in the spatial averaging; (c) a synthesis step, where a clutter covariance matrix is synthesized using the estimate of the mean clutter reflectivity $\tilde{a}_{p_i}^2$ along the isoranges at the ranges of interest.

VI. END-TO-END RESULTS

The results of the method in terms of SINR losses are illustrated in Figs. 6, 7, and 8. Figures 6 and 7 present the

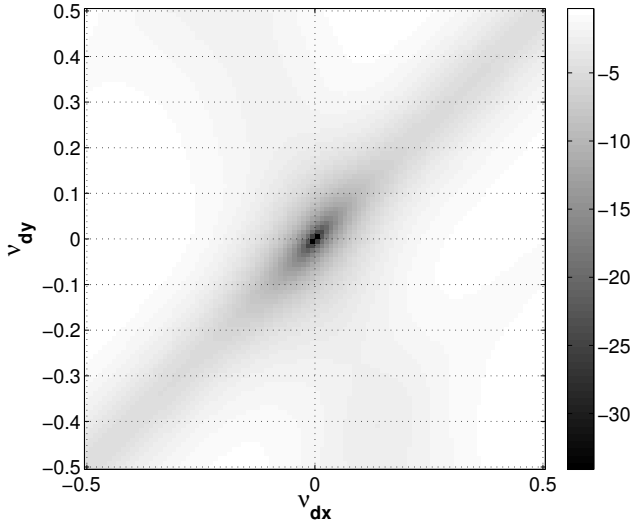


Fig. 6. SINR loss as a function of the target's velocity when considering the clairvoyant clutter covariance matrix.

SINR loss diagram in function of the 2D velocity of the target. As can be seen, there is a large “hole” at zero velocity,

corresponding to the clutter notch. Monostatic radars are only sensitive to the radial velocity component, which means that targets traveling perpendicular to the line of sight of the radar are indistinguishable from clutter. There is a similar issue with bistatic radars [23] where targets having a velocity tangential to the isorange will exhibit zero bistatic Doppler. This explains the light-gray diagonal line that corresponds to the velocities for which the target appear static to the bistatic radars Tx-Rx₂ and Tx-Rx₃. There is another – barely visible – light-gray line corresponding to the bistatic radars Tx-Rx₁. Figure 7 presents the SINR loss diagram obtained using the sample covariance matrix (with diagonal loading) as covariance matrix estimate. As can be seen from the very low value, the performance is highly degraded due to the range dependency of the clutter statistics. The diagram that is obtained (but not shown) after range dependency compensation is visually indistinguishable from the one obtained using the clairvoyant covariance matrix.

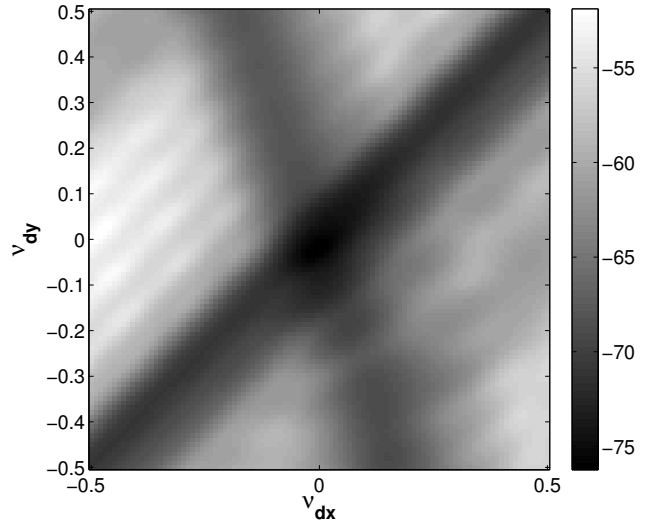


Fig. 7. SINR loss as a function of the target's velocity when considering the sample covariance matrix with diagonal loading (SCM+DL).

Finally, Fig. 8 presents a comparison of the SINR loss that would be obtained using (a) the clairvoyant covariance matrix, (b) the sample covariance matrix plus diagonal loading (SCM+DL) and (c) the proposed ML-based method as covariance matrix estimator. As can be seen, the performance of the method is almost identical to that obtained in the clairvoyant case, while the SCM+DL estimate is essentially useless.

VII. CONCLUSIONS

We considered a multistatic radar consisting of multiple mutually coherent bistatic radars. If the bistatic isoranges, along which the clutter patches are located, are disjoint, independence of the clutter signal can be assumed. In this case, the clutter covariance matrix estimation problem reduces to the independent estimation of the clutter covariance matrix of bistatic radars. This is not the case if the isoranges overlap and, generally if signals of different bistatic radars are correlated. We analyzed the range dependency of the clutter signal

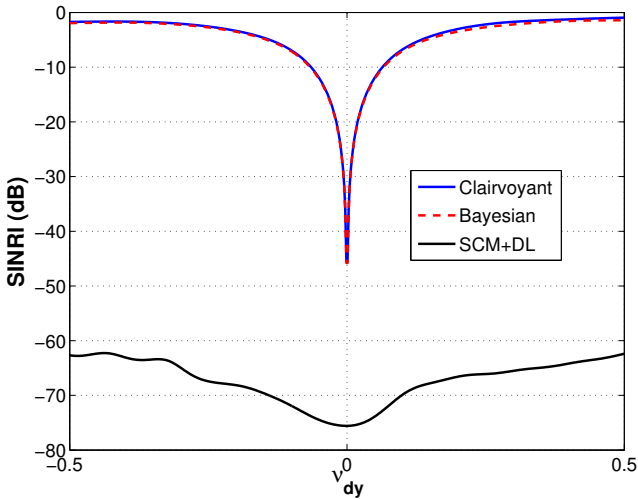


Fig. 8. SINR loss in function of the target's speed.

statistics in this case and showed that, if unaccounted for, this dependency would bias the covariance matrix estimate and severely affect the detection performance. We then proposed a generalization of a ML-based clutter reflectivity estimation method to arbitrary coherent multistatic configurations leading to a covariance matrix estimation method. The proposed method is shown to achieve excellent performance on synthetic data.

REFERENCES

- [1] D. J. Rabideau and P. Parker, "Ubiquitous MIMO multifunction digital array radar," in *Conference Record of the Thirty-Seventh Asilomar Conference on Signals, Systems and Computers*, vol. 1, pp. 1057–1064, Nov. 2003.
- [2] E. Fishler, A. Haimovich, R. Blum, D. Chizhik, L. Cimini, and R. Valenzuela, "MIMO radar: an idea whose time has come," in *Proceedings of the IEEE Radar Conference*, (Philadelphia, PA), pp. 71–76, Apr. 2004.
- [3] I. Bradaric, G. Capraro, D. D. Weiner, and M. C. Wicks, "Multistatic radar systems signal processing," in *Proceedings of the IEEE Radar Conference*, (Verona, NY), pp. 106–113, Apr. 2006.
- [4] D. R. Kirk, J. S. Bergin, P. M. Techau, and J. E. D. Carlos, "Multistatic coherent sparse aperture approach to precision target detection and engagement," in *Proceedings of the IEEE Radar Conference*, (Alexandria, VA), May 2005.
- [5] J. K. Jao, "Coherent multilateral radar processing for precise target geolocation," in *Proceedings of the IEEE Radar Conference*, (Verona, NY), pp. 325–330, Apr. 2006.
- [6] D. Bruyère and N. A. Goodman, "Performance of multistatic space-time adaptive processing," in *Proceedings of the IEEE Radar Conference*, (Verona, NY), pp. 533–538, Apr. 2006.
- [7] E. Fishler, A. Haimovich, R. S. Blum, L. Cimini, D. Chizhik, and R. A. Valenzuela, "Spatial diversity in radars — models and detection performance," *IEEE Transactions on Signal Processing*, vol. 54, pp. 823–838, Mar. 2006.
- [8] X. Neyt, J. Raout, M. Kubica, V. Kubica, S. Roques, J. G. Verly, and M. Achery, "Feasibility of STAP for passive GSM-based radar," in *Proceedings of the IEEE Radar Conference*, (Verona, NY), pp. 546–551, Apr. 2006.
- [9] J. Ward, "Space-time adaptive processing for airborne radar," Tech. Rep. 1015, MIT Lincoln Laboratory, Lexington, MA, Dec. 1994.
- [10] J. R. Guerci, *Space-Time Adaptive Processing for Radar*. Norwood, MA: Artech House, 2003.
- [11] X. Neyt, P. Ries, J. G. Verly, and F. D. Lapierre, "Registration-based range-dependence compensation method for conformal-array STAP," in *Proc. Adaptive Sensor Array Processing (ASAP) Workshop*, (MIT Lincoln Laboratory, Lexington, MA), June 2005.
- [12] X. Neyt, J. G. Verly, and M. Achery, "Range-dependence issues in multistatic STAP-based radar," in *Proceedings of the Fourth IEEE Workshop on Sensor Array and Multi-channel Processing (SAM'06)*, (Waltham, MA), July 2006.
- [13] R. Klemm, *Principles of space-time adaptive processing*. UK: The Institution of Electrical Engineers (IEE), 2002.
- [14] X. Neyt, M. Achery, and J. G. Verly, "Maximum likelihood range dependence compensation for STAP," in *Proceedings of the IEEE Conference on Acoustics, Speech and Signal Processing*, (Honolulu, HI), Apr. 2007.
- [15] M. Skolnik, *Radar handbook*. NY: McGraw-Hill, 1990.
- [16] C. Oliver and S. Quegan, *Understanding Synthetic Aperture Radar Images*. SciTech, 2004.
- [17] A. G. Jaffer, B. Himed, and P. T. Ho, "Estimation of range-dependent clutter covariance by configuration system parameter estimation," in *Proceedings of the IEEE Radar Conference*, (Arlington, VA), pp. 596–601, May 2005.
- [18] J. S. Lee, "Refined filtering of image noise using local statistics," *Computer Graphics and Image Processing*, vol. 15, pp. 380–389, 1981.
- [19] Y. Oh, K. Sarabandi, and F. T. Ulaby, "An empirical model and an inversion technique for radar scattering from bare soil surfaces," vol. 30, pp. 370–381, Mar. 1992.
- [20] A. Cavanié, "An empirical C-band backscatter model over arctic sea ice from ERS-1 AMI-wind data," in *Proc. of a Joint ESA-Eumetsat Workshop on Emerging Scatterometer Applications*, (Noordwijk, The Netherlands), pp. 99–106, ESTEC, Nov. 1995.
- [21] K. M. Golden, D. Borup, M. Cheney, E. Cherkaeva, M. S. Dawson, K.-H. Ding, A. K. Fung, D. Isaacson, S. A. Johnson, A. K. Jordan, J. A. Kong, R. Kwok, S. V. Nghiem, R. G. Onstott, J. Sylvester, D. P. Winebrenner, and I. H. H. Zabel, "Inverse electromagnetic scattering models for sea ice," *IEEE Transactions on Geoscience and Remote Sensing*, vol. 36, pp. 1675–1703, Sept. 1998.
- [22] H. Hersbach, A. Stoffelen, and S. D. Haan, "The improved C-band geophysical model function CMOD5," in *Proceedings of the Envisat Symposium*, (Salzburg, Austria), Sept. 2004.
- [23] N. J. Willis, *Bistatic Radar*. Norwood, MA: Artech House, 1991.